ISSN 1392-1320 MATERIALS SCIENCE (MEDŽIAGOTYRA). Vol. XX, No. X. 2027

Numerical Simulation of the Horizontal Continuous Casting Process for Cu-0.8Cr Alloy

Siming HUA [1, 2]*, Kai LI [1]

[1] *China Railway Construction Electrification Bureau Group Co., Ltd., No.29 Shijingshan Road, Shijingshan District, Beijing 100043, China*
[2] *University of Science and Technology Beijing, No.30 Xueyuan Road, Haidian District, Beijing 100080, China*

http://doi.org/10.5755/j02.ms.43718

Received 1 December 2025; accepted 4 February 2026

To explore the influence of horizontal continuous casting parameters on Cu-0.8Cr alloy casting, modeling and analysis were carried out using ProCAST software. The results showed that casting speed had the greatest effect on liquid core length, followed by casting temperature and the primary cooling water flow rate, while the influence of the secondary cooling water flow rate was relatively weak. For billets with diameters of 14 and 21 mm, the optimal process conditions were a casting temperature of 1180 °C, a casting speed of 1400 mm/min, a primary cooling water flow rate of 36 L/min, and a secondary cooling water flow rate of 16 L/min. For billets with a diameter of 28 mm, the optimal process conditions were a casting temperature of 1180 °C, a casting speed of 600 mm/min, a primary cooling water flow rate of 36 L/min, and a secondary cooling water flow rate of 16 L/min.

Keywords: Cu-0.8Cr alloy, horizontal continuous casting, numerical simulation, temperature field, liquid core length.

1. INTRODUCTION

Age-hardened Cu-Cr alloys are among the most promising materials for lead frames [1, 2], high-speed railway contact wires [3] and electronic connectors [4]. Horizontal continuous casting is well suited for producing such alloys, offering both low cost and high billet quality [5, 6]. During this process, the molten copper alloy solidifies in the crystallizer. However, direct observation and measurement of temperature evolution in the melt, the crystallizer, and the growing solid shell are difficult. Producing cast billets of high quality often requires multiple experimental trials, which are expensive and time-consuming. To address these challenges, researchers have increasingly applied numerical simulation to study horizontal continuous casting of copper and its alloys. Simulation helps clarify this "black box" process while reducing experimental cycles and costs.

Li et al. [7] have investigated the effects of pouring temperature, cooling intensity, and casting speed on the mushy zone width and liquid core depth of BFe30-1-1 alloy tube billets using numerical simulation and have experimentally verified the numerical results. Sha et al. [8] have built a three-dimensional model for the electromagnetic stirring of round copper billets in horizontal continuous casting. Their study has shown that with a current intensity of 40 A and a frequency of 10 Hz, the maximum magnetic flux density and time-averaged electromagnetic force on the billet surface are 100 mT and 72×10^{-3} N, respectively. Cui and Zhang, et al. [9, 10] have investigated the effects of electromagnetic stirring on microstructural morphology and liquid crater depth during solidification. They have demonstrated that electromagnetic stirring induces forced convection in the molten metal, which not only accelerates liquid-phase cooling but also modifies the primary solidification structure. As a consequence, the liquid crater depth decreases, columnar grain growth is inhibited, and the fraction of equiaxed grains increases.

Yi et al. [11] have examined temperature and structural evolution during the solidification of pipe blanks in horizontal continuous casting molds. In addition, they have analyzed the relationship between cooling water flow rate, withdrawal speed, casting temperature, and the morphology of the liquid sump in the crystallizer. Kim et al. [12] have analyzed the effects of process parameters such as initial melt temperature and casting speed on the grain structure of Cu-22 wt.% Sn alloy slabs. Their results have shown that casting speed is a critical factor influencing the angle between columnar grains and the casting direction.

In the present study, a solidification model for horizontal continuous casting of a Cu-Cr alloy was established without electromagnetic stirring, providing a research foundation for subsequent numerical modeling that incorporated electromagnetic stirring.

To reduce test costs and provide guidance for debugging horizontal continuous casting processes, the horizontal continuous casting of Cu-0.8Cr alloy was modeled and analyzed in the present study using ProCAST software. In addition, the present study examined the influence of casting temperature, casting speed, and primary and secondary cooling water flow rates on the liquid core length and the temperature field of the copper mold.

2. MODEL AND BOUNDARY CONDITIONS

2.1. Geometric model and meshing

Fig. 1 shows a schematic diagram of horizontal continuous casting for the Cu-0.8Cr alloy. In this process,

* Corresponding author: S. Hua
E-mail: *huasiming.dqh@crcc.cn*

electrolytic copper and Cu15Cr alloy were melted in an induction furnace and then entered furnace (1) to form molten alloy (2). During horizontal continuous casting, the molten Cu-0.8Cr alloy was continuously fed into the graphite mold (6), where it was cooled by the cooling system (5, 7, 8, 9), and solidified into a continuous copper alloy bar (10). The surface of the molten alloy was covered with graphite flakes (3), and the alloy liquid was stirred by the electromagnetic stirrer (4).

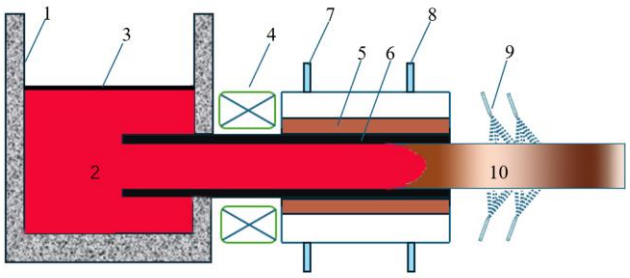

Fig. 1. Schematic diagram of horizontal continuous casting: 1 – heat-insulated furnace; 2 – copper alloy melt; 3 – graphite flakes; 4 – electromagnetic stirrer; 5 – copper mold; 6 – graphite mold; 7 – primary cooling water inlet; 8 – primary cooling water outlet; 9 – secondary cooling water; 10 – copper alloy bar

In the above process, the temperature of the copper alloy melt, the cooling system, and the continuous casting speed had an impact on the quality of the billets. To comprehensively investigate the influence of these factors, a simplified horizontal continuous casting model was established. The model included the Cu-0.8 Cr alloy melt, furnace lining, graphite mold, water-cooled copper sleeve, billet, and secondary cooling zone, and was used to study the solidification and cooling process of the Cu-0.8 Cr alloy.

Because of the axial symmetry of the research object, a half three-dimensional symmetrical geometric model was established to save computation time, as shown in Fig. 2.

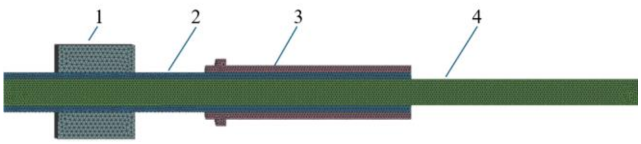

Fig. 2. Geometric model diagram of horizontal continuous casting: 1 – refractory lining; 2 – graphite mold; 3 – copper mold; 4 – copper alloy bar

Since the horizontal continuous casting solidification process involved many factors, the physical model was partially simplified for simulation, and the effect of the electromagnetic stirrer was not considered. The geometric model had a total length of 500 mm, with the graphite mold measuring 320 mm and the copper mold for primary cooling water measuring 160 mm. The billet diameters were set at 14, 21, and 28 mm. All models were created in accordance with the actual geometric dimensions of the crystallizer. The three-dimensional model was first constructed in Unigraphics NX, and the surface and volume meshes were generated using Meshcast software.

To minimize the influence of mesh size on the simulation results, a systematic grid convergence analysis was performed in the present study. While maintaining consistent geometric and solution parameters, three sets of structured grids, coarse, medium, and fine, were generated with element sizes of 4, 2, and 1 mm, corresponding to element counts of 6.54×10^4, 2.15×10^5, and 1.38×10^6, respectively. The solid fraction was selected as the convergence criterion. The calculated results for the three grid sets were 62.6 %, 62.1 %, and 62.0 %, respectively. By plotting the relationship curve between solid fraction and grid size, it was observed that the curve gradually flattened, indicating that the results had converged. Based on this analysis, the 2 mm mesh was selected for subsequent simulation calculations in this study.

The residual threshold was defined as less than 1×10^{-4}, with a temperature convergence criterion of 1 K and a temperature relaxation factor of 1.0. The calculation results were examined, and it was found that the residuals showed a monotonic decreasing trend without any rebound. Furthermore, with a fixed mesh size of 2 mm and a constant physical model, the time step was progressively increased while the results were monitored, and no oscillations were detected. Overall, the numerical calculations in the present study exhibited good stability and convergence.

2.2. Physical properties

Table 1 lists the physical properties of Cu-0.8Cr alloy relevant for the present study. The enthalpy and density are functions of temperature. The mass fractions of Cr and Cu were entered into ProCAST, and the physical properties of the Cu-0.8Cr alloy were obtained from the ProCAST calculations, as listed in Table 1.

Table 1. Physical properties of Cu-0.8Cr alloy

Parameters	Value
Density at 25 ℃, kg/m^3	8919
Density at 1078 ℃, kg/m^3	8011
Specific heat, J/kg℃	385
Enthalpy at 25 ℃, kJ/kg	3.094
Enthalpy at 1078℃, kJ/kg	663.73
Melting point, ℃	1078
Bar diameter, mm	14/21/28
Bar length, mm	500

2.3. Initial and boundary conditions

The initial temperature of the graphite mold and the refractory furnace lining was set to 200 °C. The initial temperature of the copper mold was set to 30 °C. The initial temperature of the Cu-0.8Cr alloy bar billet was taken as the casting temperature.

Fig. 3 shows a schematic of the boundary and interface conditions. Boundary 1 included the crystallizer inlet, the part of the graphite mold extending into the molten copper alloy, and the furnace lining in contact with the melt (Fig. 3).

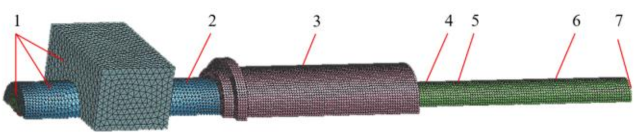

Fig. 3. Schematic diagram of the boundary and interface conditions

This boundary was defined as a constant-temperature boundary, with a value equal to the pouring temperature of the Cu-0.8Cr alloy. Boundary 2 was defined as the contact area between the graphite mold and air. Since the furnace shell temperature during the normal production process was 200 ℃, the ambient temperature of this boundary was set to the same temperature. Heat transfer at this boundary was assumed to occur through thermal radiation and natural convection. According to other authors [13, 21], the emissivity coefficient of radiative heat transfer was taken as 0.9, and the convective heat transfer coefficient was taken as 6.5 W/(m²·K).

Boundary 3 was defined as the interface between the cooling water and the copper mold, where the heat transfer coefficient and the primary cooling water temperature were specified. Boundary 4 was located between the primary and secondary cooling zones of the casting billet, where the surface was splashed by secondary cooling water. Therefore, Boundary 4 was assumed to involve both radiation and convective heat transfer [14], and the heat transfer coefficient was set to 5000 W/(m²·K) after calculation. Boundary 5 was defined as the secondary cooling water area and was modeled as jet impingement with forced convective heat transfer.

Boundary 6 was defined as the contact interface between the Cu-0.8Cr alloy bar and air. The boundary condition was specified as natural convective heat transfer with a coefficient of 586 W/(m²·K). Since the heat conducted through the cross-section of the continuous casting billet was much smaller than that conducted through its axial surface, Boundary 7 was defined as an adiabatic boundary.

2.4. Calculation of heat transfer coefficient

2.4.1. The heat transfer coefficient of the primary cooling zone

As shown in Fig. 3, the boundary of the primary cooling zone was defined as Interface 3, and its heat transfer coefficient was calculated using Eq. 1 [15]:

$$h_{c1} = \frac{\lambda N_u}{d_e}, \tag{1}$$

where h_{c1} is the interfacial heat transfer coefficient of the primary cooling water; N_u is the Nusselt number; λ is the thermal conductivity of water; d_e is the equivalent diameter. In the present study, the equivalent diameter was set to 20 mm. N_u was calculated according to Eq. 2 [16]:

$$N_u = 0.023 {R_e}^{0.8} P_r^n, \tag{2}$$

where for heating the fluid, $n = 0.4$; R_e is the Reynolds number; P_r is the Prandtl number.

Assuming an average inlet and outlet temperature of 30 °C for the primary cooling water, the value of P_r in Eq. 2 was 5.42. R_e is a parameter that varies with liquid flow velocity (u), equivalent diameter (d), liquid density (ρ), and dynamic viscosity (η), as defined in Eq. 3 [16].

$$R_e = \frac{ud\rho}{\eta}. \tag{3}$$

2.4.2. The heat transfer coefficient of the second cooling zone

As shown in Fig. 3, Boundary 5 was defined as the secondary cooling water boundary. To achieve strong heat exchange, the secondary cooling water was sprayed onto the surface of the billet through a circular nozzle. The heat transfer coefficient of the secondary cooling zone was calculated using Eq. 4 [17], which describes the average heat transfer characteristics of circular nozzle jet flow:

As shown in Fig. 3, Boundary 5 was defined as the secondary cooling water boundary. To achieve strong heat exchange, the secondary cooling water was sprayed onto the surface of the billet through a circular nozzle. The heat transfer coefficient of the secondary cooling zone was calculated using Eq. 4 [17], which describes the average heat transfer characteristics of circular nozzle jet flow:

$$h_{c2} = \frac{\lambda N_u}{r}, \tag{4}$$

where h_{c2} is the heat transfer coefficient at the secondary cooling water; N_u is the Nusselt number; λ is the thermal conductivity of water; r is the characteristic length.

The Nusselt number was calculated according to Eq. 5 [17]:

$$N_u = 2{R_{eD}}^{0.5} P_r^{0.42} \left(1 + 0.005{R_{eD}}^{0.55}\right)^{0.5} \times \frac{1 - 1.1 D/r}{1 + 0.1(H/D - 6) D/r} D/r, \tag{5}$$

where R_{eD} is the Reynolds number; P_r is the Prandtl number (0.86); H is the distance from the nozzle to the casting billet; D is the nozzle diameter; r is the characteristic length.

Assuming a characteristic temperature of 250 °C for the secondary cooling water, the value of P_r in Eq. 5 was 0.86. R_{eD} is a parameter that varies with the average jet velocity (u) at the nozzle outlet, nozzle diameter (D), and fluid kinematic viscosity (v), as specified in Eq. 6 [17].

$$R_{eD} = \frac{uD}{v}. \tag{6}$$

2.5. Interfacial heat transfer coefficient

Fig. 4 shows a schematic diagram of the interface conditions of the geometric model. The contact interface between the graphite mold and the refractory furnace lining (resin sand) was defined as Interface I. Referring to the test method in the ASTM 5470-17 [18], the interfacial heat transfer coefficient between the graphite mold and resin sand was measured as 1000 W/(m²·K) in the present study.

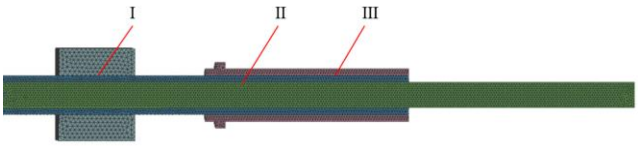

Fig. 4. Schematic diagram of interface conditions

The contact interface between the molten alloy and the graphite mold was defined as Interface II. According to previous research [19], the general range of heat transfer coefficients at the liquid metal/mold interface was 10,000 – 20,000 W/(m²·K). Therefore, in the present study, the interfacial heat transfer coefficient was set to

15,000 W/(m²·K) for the interface between molten Cu-0.8Cr alloy and the graphite mold.

The contact interface between the red copper sleeve and the graphite mold was defined as Interface III, with close contact between the two components. Based on actual measurements and calculations, Liu et al. [20] have reported that when copper is in close contact with graphite molds, the heat transfer coefficient ranges from 2400 to 2600 W/(m² K). Accordingly, in the present study, the heat transfer coefficient of interface III was set to 2500 W/(m² K).

The quality of billets produced by horizontal continuous casting was influenced by many factors, including pouring temperature, billet withdrawal speed, primary and secondary cooling water flow rates, and billet diameter. Because of these multiple influences, studying the relationship between billet quality and process parameters often requires multiple experiments [21]. Orthogonal experimental design, a tool for addressing multifactor and multilevel problems, was applied to efficiently select representative trials through orthogonality.

In the present study, an orthogonal method was used to design a four-factor, two-level experiment with a central point. Based on production experience, four factors were selected: casting temperature, casting speed, primary cooling water flow rate, and secondary cooling water flow rate. Two levels of casting temperatures were chosen: 1180 and 1215 °C. Casting speeds were set at 600 and 1400 mm·min^{-1}. Flow rates of primary and secondary cooling water were set to 16 and 36 L·min^{-1}. The models were analyzed for billet diameters of 14, 21, and 32 mm.

3. ANALYSIS OF SIMULATED RESULTS

3.1. Analysis of influencing factors on the liquid core length

The casting temperature, casting speed, and the flow rates of primary and secondary cooling water were identified as important factors affecting billet quality and production efficiency in horizontal continuous casting. The distance from the liquid level in the crystallizer to the point where the billet center completely solidifies is defined as the liquid core length [22]. This parameter directly reflects the cooling condition of the billet and the suitability of the continuous casting process. Investigation of the liquid core length is therefore important for balancing production efficiency and billet quality. In the present study, orthogonal experiments were carried out to examine how these four factors influenced the continuous casting of Cu-0.8Cr alloy. The numerical simulation results for the liquid core length at different billet diameters and process parameters are summarized in Table 2. The results showed the following trends: when the billet diameter was 14 mm, the liquid core length varied between 16.68 and 20.93 mm; when the billet diameter was 21 mm, it ranged from 17.91 mm to 24.35 mm; and when the billet diameter was 28 mm, it changed between 20.90 and 32.42 mm. Thus, a larger billet diameter resulted in a greater variation of liquid core length.

Table 3 presents the main effects of each process parameter at different billet diameters. These values represented the independent influence of different parameter levels on the liquid core length, reflecting the overall effect when each parameter acted alone. A larger main effect value indicated a greater impact of the parameter change on the experimental results. When the billet diameter was 14 mm, the main effect of casting temperature was 0.70 mm, casting speed was 2.59 mm, the primary cooling water flow rate was -0.94 mm, and the secondary cooling water flow rate was -0.02 mm. These results indicated that casting speed had the greatest effect on the liquid core length, followed by the primary cooling water flow rate and casting temperature, while the secondary cooling water flow rate had almost no effect.

When the billet diameters were 21 and 28 mm, the main effects of casting temperature were 1.32 and 3.29 mm, respectively. The main effects of casting speed were 3.79 and 7.01 mm, respectively. The main effects of the primary cooling water flow rate were -1.34 and -1.19 mm, respectively. The main effects of the secondary cooling water flow rate were 0.03 and 0.74 mm, respectively.

Table 2. Numerical simulation results for different process parameters and billet diameters

No.	Casting temperature, ℃	Casting speed, mm/min	Primary cooling flow rate, L/min	Secondary cooling flow rate, L/min	Liquid core length, mm		
					Ø14	Ø21	Ø28
1	1180	600	16	16	16.91	18.60	20.90
2	1280	1400	36	36	19.24	22.40	30.76
3	1180	1400	16	36	19.73	22.33	29.22
4	1280	1400	16	16	20.93	24.35	32.42
5	1180	600	36	36	16.68	17.91	21.67
6	1180	1400	36	16	18.91	20.91	27.48
7	1280	600	16	36	17.94	19.81	25.69
8	1280	600	36	16	16.92	18.49	23.56

Table 3. Main effects of process parameters at different billet diameters

Billet diameter, mm	Main effects of process parameters			
	Casting temperature, ℃	Casting speed, mm/min	Primary cooling flow rate, L/min	Secondary cooling flow rate, L/min
14	0.70	2.59	-0.94	-0.02
21	1.32	3.79	-1.34	0.03
28	3.29	7.01	-1.19	0.74

These results indicated that casting speed had the greatest influence on the liquid core length, followed by casting temperature, while the flow rates of primary and secondary cooling water had smaller effects. Fig. 5 shows the main effect diagrams at different billet diameters and process parameters. The results indicated that the liquid core length increased as the casting temperature and casting speed rose. For billet diameters of 14 and 21 mm, increases in the flow rates of primary and secondary cooling water shortened the liquid sump length. For a bar diameter of 28 mm, an increase in the primary cooling water flow rate shortened the liquid core length, while an increase in the secondary cooling water flow rate extended it. These results indicated that for larger billet diameters, a higher flow rate of secondary cooling water accelerated external cooling, leading to excessive billet shrinkage. This premature shrinkage caused the early formation of an air gap between the solidified shell and the crystallizer inner wall, which was unfavorable for heat transfer. In addition, the solid billet shell reduced the heat transfer efficiency of the metal [23], preventing complete solidification at the billet center and thereby resulting in an increased liquid core length.

3.2. Temperature field analysis of the copper mold

Fig. 6 shows the temperature contour maps of the copper mold under different billet diameters and processes, where No. 1 to No. 8 correspond to the process numbers in Table 2. The results indicated that the temperature distributions of the copper sleeve varied significantly with process conditions. For example, for a billet diameter of 28 mm, the sleeve temperature under process No. 1 was higher than 380 °C, whereas under process No. 8 was lower than 380 °C. An increase in the primary cooling water flow rate resulted in a lower sleeve temperature. Across different billet diameters, the temperature distributions of the copper sleeve were not completely consistent. Larger billet diameters led to better temperature uniformity and higher minimum temperatures. For instance, with a diameter of 14 mm under process No. 1, the sleeve temperature ranged from 100 to 750 °C, with a minimum of approximately 165 °C.

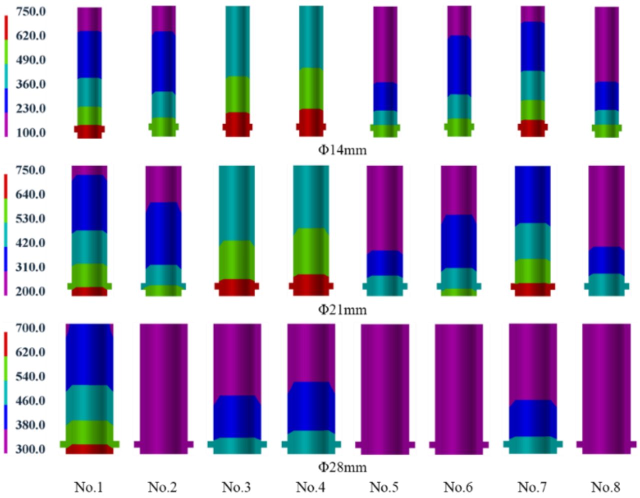

Fig. 6. Temperature contour maps of the copper sleeve at different billet diameters and process parameters

With a diameter of 28 mm under the same process, the sleeve temperature ranged from 300 to 700 °C, showing relatively uniform distribution and a minimum of about 340 °C. Overall, when the billet diameter was 14 mm, the maximum sleeve temperatures across processes were 750 and 620 °C. When the diameter was 21 mm, the maximum sleeve temperatures were 750, 640, and 530 °C. When the diameter was 28 mm, the maximum sleeve temperatures were 700, 540, and 380 °C.

Following the selection of Process Scheme 1, based on the actual conditions of the mold for the 28 mm billet in the industrial setting, 1 mm holes were drilled in the mold jacket.

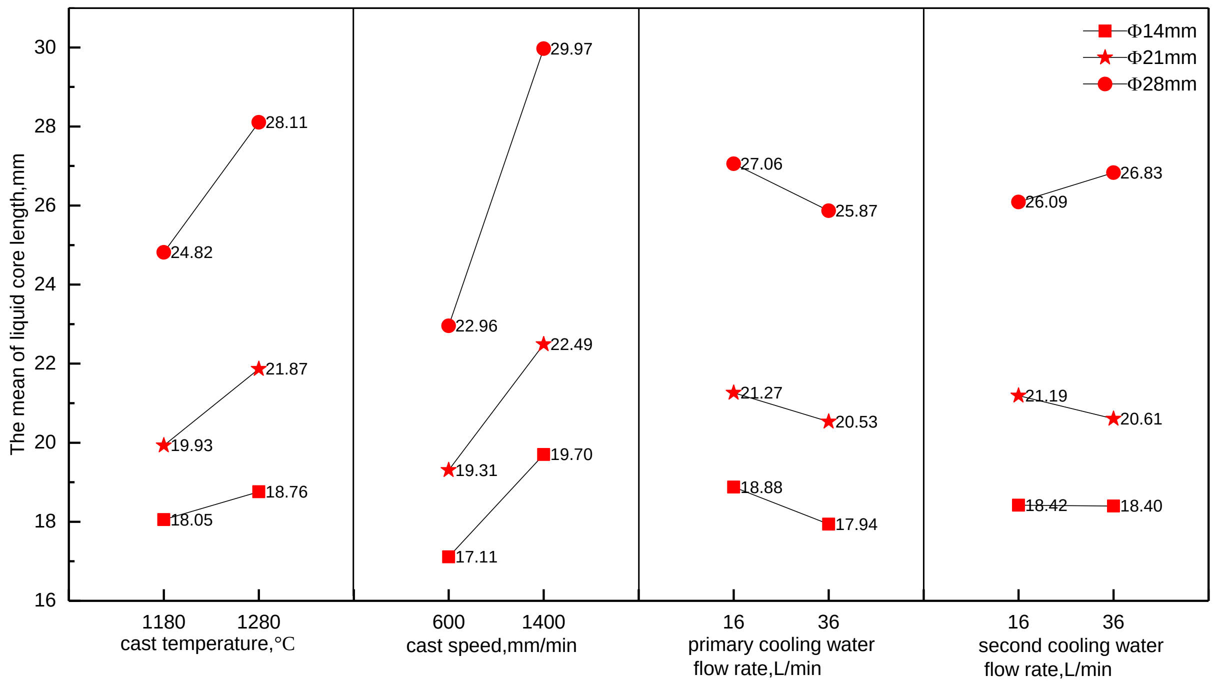

Fig. 5. Main effects diagrams of process parameters at different billet diameters

K-type thermocouples were fixed to the copper jacket at three points (A, B, and C), as shown in Fig. 7. Table 4 presents the average deviation between the simulated and measured temperatures at these three monitoring points under steady-state conditions. The absolute error at each point was controlled within 10 – 30 ℃, and the relative error remained below 5 %, indicating that the simulation results showed good agreement with the experimental measurements.

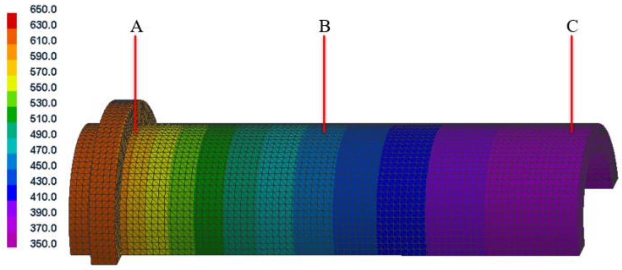

Fig. 7. Schematic diagram of thermocouple layout

Table 4. Comparison between measured temperatures and simulation results at each monitoring point

Position	Measured value, ℃	Simulation result, ℃	Absolute error, ℃	Relative error, %
A	646.5	619.6	26.9	4.2
B	456.8	441.5	15.3	3.3
C	390.7	378.8	11.9	3.0

3.3. Temperature analysis of the casting billet

Fig. 8 shows billet temperature at different billet diameters and process parameters. Fig. 8 a presents the central temperature of the casting billet at the crystallizer outlet for various diameters and processes, where processes No. 1 through No. 8 correspond to those listed in Table 2. For a billet diameter of 28 mm, the central temperature at the crystallizer outlet exceeded 960 °C under the process conditions No. 2 – 4 and No. 6. Fig. 7 b presents the maximum temperature difference between the interior and exterior of the casting billet under different diameters and processes, again corresponding to the process numbers in Table 2. The results showed that when the billet diameter was 14 mm, the internal-external temperature difference was relatively small, fluctuating between 29 and 46 °C. When the billet diameters were 21 and 28 mm, the internal and external temperature differences of the billet are relatively close, the temperature differences were relatively close, with the maximum difference of 134 °C occurring under process No. 4.

The process parameters for No. 4 were as follows: casting temperature 1280 °C, casting speed 1400 mm/min, primary cooling water flow rate 16 L/min, and secondary cooling water flow rate 16 L/min. Under these conditions, the internal-to-external temperature difference for the 21 mm diameter billet was approximately 50 °C, while that for the 28 mm diameter billet reached about 135 °C. This indicated that, under the given process conditions, the 28 mm diameter billet required a higher cooling water flow rate compared to the 21 mm diameter billet. The cooling water flow rate applied in this process was insufficient to ensure stable continuous casting, which was corroborated by the surface cracks observed in the billet produced under Process A as discussed in the subsequent section.

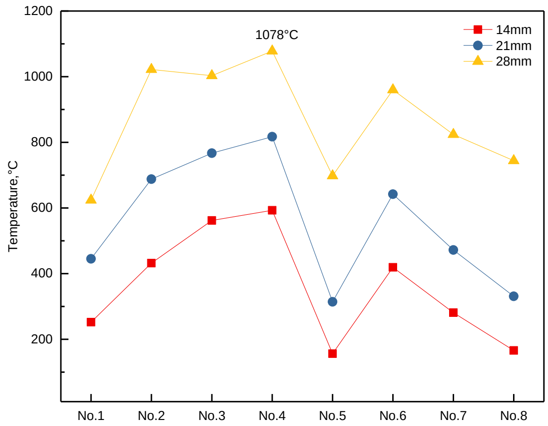

a

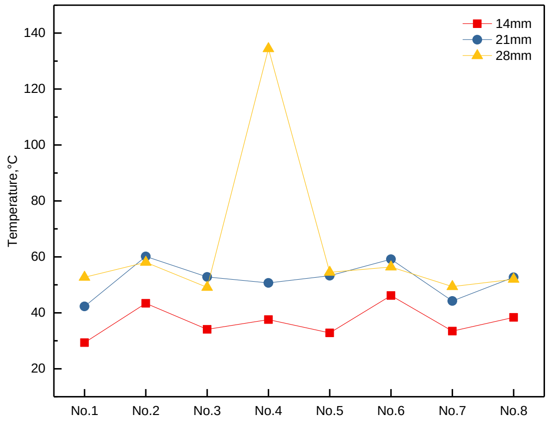

b

Fig. 8. Temperature of the casting billet at different billet diameters and process parameters: a – central temperature of the casting billet at the crystallizer outlet; b – maximum temperature difference between the casting billet interior and exterior

4. DISCUSSION

Raising the casting speed improves the efficiency of horizontal continuous casting. An increase in casting speed shortens the residence time of liquid copper in the graphite mold, extends the liquid core length of the billet, raises the billet shell temperature, and reduces its fracture strength. When the interfacial friction between the graphite mold and the billet shell exceeds the fracture resistance of the solidified shell, surface defects such as cracks may develop. As casting speed increases, the surface quality of the billet first improves and then deteriorates [24]. In addition, excessively high casting speeds cause segregation and microstructural porosity in the billet [25]. Therefore, in actual production, the casting speed is limited by the mold, casting temperature, and cooling conditions. A critical speed exists, defined as the speed at which the billet temperature at the mold outlet equals the alloy solidus temperature [26, 27]. As shown in Fig. 7, for the billet with a diameter of 28 mm under process No. 4, the temperature at the mold outlet reached 1078 °C, which was higher than the solidus temperature (1071 °C). This result indicated that continuous casting breakage occurred under this condition. A longer liquid core length increased the resistance to molten copper feeding, which could lead to shrinkage cavities or porosity defects and raised casting stress, thereby causing center cracks in the billet. For this reason, in actual production, the liquid sump morphology of the casting billet is expected to remain flat [28].

The quality of cast billets was significantly affected by casting temperature. A relatively high casting temperature allowed for higher casting speed and improved production efficiency. At lower casting temperatures, the alloy liquid at the crystallization front solidified more readily during cooling, which reduced fluidity and hindered mold filling. As the casting temperature increased, the alloy fluidity improved, the attractive forces between atoms weakened, and melt viscosity decreased, all of which promoted better melt fluidity [29]. However, excessively high casting temperatures caused greater alloy shrinkage and increased gas solubility in the liquid metal, which led to defects such as porosity and blowholes [30]. For Cu-Cr alloys, the casting temperature is generally around 1200 °C [31, 32]. Because the melt fluidity of Cu-Cr alloys is relatively low, the casting temperature should be maintained as high as feasible within the safe processing range.

According to heat transfer theory [33], when the cooling structure is fixed, the effect of increasing the cooling water flow rate on solidification is not linear. Once the flow rate exceeds a certain range, further increases do not improve heat exchange efficiency, making it difficult to cool the molten copper effectively during high-speed casting [33]. Beyond this limit, a higher cooling water flow rate does not enhance cooling intensity; instead, it adversely affects the billet quality [34].

The strength of pure copper is 190 MPa at 500 °C, 145 MPa at 600 °C, 90 MPa at 700 °C, and 80 MPa at 750 °C [35, 36]. Based on the analysis of Fig. 6, for a billet diameter of 14 mm, the temperature in the red area of the copper sleeve under processes No. 1, 3, 4, and 7 ranged from 620 to 750 °C. For a billet diameter of 21 mm, the temperature in the red area under the same processes ranged from 640 to 750 °C. For a billet diameter of 28 mm, the temperature in the red area under process No. 1 was between 620 and 700 °C. Under these process conditions, some regions of the copper sleeve may be exposed to high temperatures, resulting in reduced strength (< 145 MPa). During long-term continuous casting, exposure of the mold to both vibration and high temperatures makes the copper sleeve prone to damage and deformation, which in turn leads to instability in the continuous casting process.

When molten copper solidifies, a temperature gradient develops between the outer shell and the billet center. A corresponding density gradient is also formed from the surface to the core. Changes in the temperature gradient alter the density gradient, disrupt the original stress balance in the billet, and generate internal thermal stresses. With enhanced cooling, the temperature gradient between the surface shell and the billet center increases, and the density gradient increases as well. The billet surface shell is subjected to tensile stress, while the solidification front experiences compressive stress. This imbalance may cause cracks in regions with weak dendritic bonding. When cooling is weak or completed, the surface temperature of the billet rises, and the billet shell expands due to reheating. Under these conditions, the billet surface shell is under compressive stress, while the billet interior is subjected to tensile stress. This stress state readily leads to internal crack defects, which in turn deteriorate billet quality [37, 38].

Based on the above analysis, for billets with diameters of 14 and 21 mm, the copper sleeve temperature was maintained lower than 620 °C. Considering the low internal-external temperature difference of the billet, high manufacturing efficiency, casting temperature near 1200 °C, and reduced cooling water consumption, the process conditions of 1180 °C casting temperature, 1400 mm/min casting speed, 36 L/min primary cooling water flow rate, and 16 L/min secondary cooling water flow rate (process No. 6, Table 2) were determined as optimal. For billets with a diameter of 28 mm, the copper sleeve temperature was kept below 540 °C. Under this condition, the corresponding process was found to be more suitable. Additionally, when accounting for the low internal-external temperature difference of the billet, high manufacturing efficiency, casting temperature near 1200 °C, a crystallizer outlet temperature below 900 °C, and reduced cooling water consumption, the process conditions of 1180 °C casting temperature, 600 mm/min casting speed, 36 L/min primary cooling water flow rate, and 16 L/min secondary cooling water flow rate were considered optimal.

Based on the above results, two schemes were designed to test horizontal continuous casting of 28-mm billets. Scheme B was a process with favorable outcomes based on numerical simulation results, whereas Scheme A corresponded to a process with less favorable performance. The process parameters of Scheme A were: casting temperature 1280 °C, casting speed 1400 mm/min, primary cooling water flow rate 36 L/min, and secondary cooling water flow rate 16 L/min. The parameters of Scheme B were: casting temperature 1180 °C, casting speed 600 mm/min, primary cooling water flow rate 16 L/min, and secondary cooling water flow rate 16 L/min. Fig. 9 shows the appearance and longitudinal cross-sectional metallography of the billets prepared by the two test schemes.

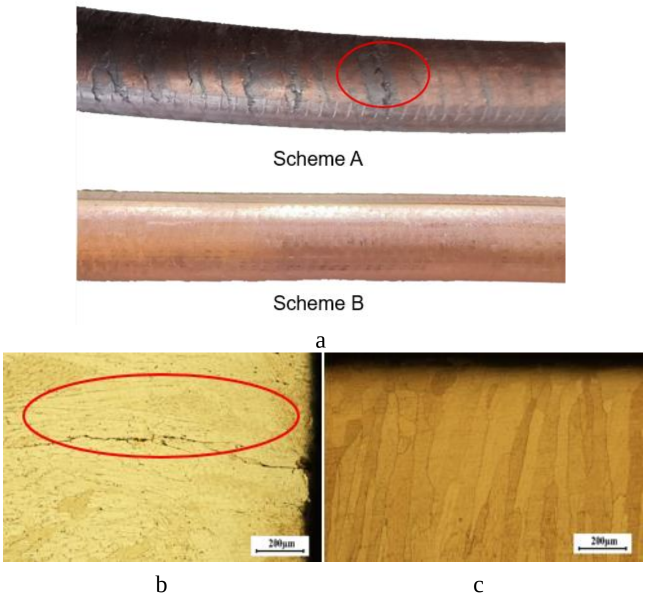

Fig. 9. Surface quality and microstructure of billets under different schemes

It can be observed that the billet prepared by Scheme A has poor surface quality, with significant defects (the area within the red circle in Fig. 9 a), and its surface color is relatively dark. This indicates that the surface temperature of the continuous casting billet was relatively high when it exited the mold. In addition, the microstructure of the billet also had penetrating cracks (the area within the red circle in Fig. 9 b), which extended approximately 1200 microns into the billet. In contrast, the billet prepared by Scheme B has a smooth surface with a bright yellow color, which suggests that the surface temperature of the continuous casting billet was relatively low when it exited the mold, and there were no cracks in its microstructure (Fig. 9 c).

5. CONCLUSIONS

1. Within the ranges of 1180 – 1280 °C casting temperature, 600 – 1400 mm/min casting speed, and 16 – 36 L/min primary and secondary cooling water flow rates, the continuous casting speed had the greatest impact on the liquid sump length. The casting temperature and primary cooling water flow rate had smaller effects, while the secondary cooling water flow rate had the least influence.
2. The simulation showed that under different process conditions, the temperature distributions of the copper sleeve varied significantly. Therefore, it was recommended to select a process with a lower copper sleeve temperature. In addition, the internal-external temperature difference of the billet and the crystallizer outlet temperature were considered effective criteria for evaluating the stability of the continuous casting process.
3. A comprehensive evaluation of the billet temperature at the crystallizer outlet, the internal-external temperature difference of the billet, the copper sleeve temperature, and the casting process parameters showed that for billets with diameters of 14 and 21 mm, the optimal process conditions were a casting temperature of 1180 °C, a casting speed of 1400 mm/min, a primary cooling water flow rate of 36 L/min, and a secondary cooling water flow rate of 16 L/min (process No. 6). For the billets with a diameter of 28 mm, the optimal process conditions were a casting temperature of 1180 °C, a casting speed of 600 mm/min, a primary cooling water flow rate of 36 L/min, and a secondary cooling water flow rate of 16 L/min.

Acknowledgments

This study was conducted with the support from Major Science and Technology Special Project of China Railway Construction Corporation Limited (2023-Z01).

REFERENCES

1. **Xia, C.D., Zhang, W., Kang, Z.Y., Wu, Y.F., Zhang, R., Xu, G.Y., Wang, M.P.** High Strength and High Electrical Conductivity Cu-Cr System Alloys Manufactured by Hot Rolling-quenching Process and Thermomechanical Treatments *Materials Science & Engineering, A* 538 2012: pp. 295 – 301. https://doi.org/10.1016/j.msea.2012.01.047
2. **Luo, X.Y., Tang, X.C., Kuang, C., Zhang, Z.J., Zhou, W.L.** Research Status and Progress of High Strength and High Conductivity Cu-Cr Alloys *China Metallurgy* 33 (7) 2023: pp. 10 – 20. https://doi.org/10.13228/j.boyuan.issn1006-9356.20230121
3. **Yuan, Y., Li, Z., Xiao, Z., Zhao, Z.Q., Yang, Z.Q.** Microstructure Evolution and Properties of Cu-Cr Alloy During Continuous Extrusion Process *Journal of Alloys and Compounds* 703 2017: pp. 454 – 460. https://doi.org/10.1016/j.jallcom.2017.01.355
4. **Yang, Q., Wang, Z.L., Xiao, X.Y., Xie, J.X.** Effect of Different Solid Solution Treatments on Microstructure and Properties of Cu-Cr Alloy *The Chinese Journal of Nonferrous Metals* 34 (1) 2024: pp.89 – 99. https://doi.org/10.1016/j.phpro.2013.11.011
5. **Gu, W.** Status and Development of Horizontal Continuous Casting Machines *Steel Pipe* 1 1993: pp. 57 – 62.
6. **Luo, H.L., Feng, D., Li, S.P., Cao, X., Wang, J.T.** Numerical Simulation of Vacuum Horizontal Continuous Casting Process for Superalloy bar *Continuous Casting* 40 (2) 2015: pp. 29 – 37. https://doi.org/10.13228/j.boyuan.issn1005-4006.20140138
7. **Li, X.T., Zhao, X.W., Ma, X.R.** Numerical Simulation of Solidification Process of Horizontal Continuously Cast Bfe30-1-1 Hollow Billets *Foundry* 8 2007: pp. 841 – 844. https://doi.org/CNKI:SUN:ZZZZ.0.2007-08-018
8. **Sha, M.H., Wang, T.M., Li, J.** Numerical Simulation of Horizontal Continuous Casting Process of Round Copper Billet With Electromagnetic Stirring *International Journal of Cast Metals Research* 12 2013: pp. 197 – 202. https://doi.org/10.1179/136404611X13001912814103
9. **Cui, J., Zhang, H., Li, L., Zuo, Y., Nagaumi, H.** Electromagnetic Stirring and Low-Frequency Electromagnetic Vibration. In: Eskin, D., Mi, J. (eds) Solidification Processing of Metallic Alloys Under External Fields. Springer Series in Materials Science: SpringerCham; 2018: pp. 119 – 151. https://doi.org/10.1007/978-3-319-94842-3_4
10. **Zhang, W., Luo, S., Chen, Y., Wang, W., Zhu, M.** Numerical Simulation of Fluid Flow, Heat Transfer, Species Transfer, and Solidification In Billet Continuous Casting Mold With M-ems *Metals* 9 (1) 2019: pp. 66 – 70. https://doi.org/10.3390/met9010066
11. **Yi, H., Zhang, X.B., Yu, E.L., Lei, S., Ying, G.** Numerical Analysis of Temperature Field And Structure Field in Horizontal Continuous Casting Process For Copper Pipes *International Journal of Heat and Mass Transfer* 115 2017: pp. 294 – 306. https://doi.org/10.1016/j.ijheatmasstransfer.2017.08.037
12. **Kim, Y.Y., Kim, H.S.** Prediction of Grain Structure of Thin Bronze Slab Produced by Horizontal Continuous Casting *Metals and Materials International* 25 2019: pp. 465 – 472. https://doi.org/10.1007/s12540-018-00231-w
13. **Zhao, W., Cai, F., Cai, X., Cao, W.W.** Radiation Properties of Carbon Materials for High Temperature Furnace *Journal of Functional Materials* 42 (7) 2011: pp. 1305 – 1308. https://doi.org/CNKI:SUN:GNCL.0.2011-07-037
14. **Zhang, F.L., Zhou, Y.Q.** Experimental Study on Heat Transfer Coefficient of Water Spray Cooling in Secondary Cooling Zone of Continuous Casting *Iron and Steel* 4 1985: pp. 49 – 53.
15. **Chu, D., Ben, L.H., Wu, C.J.** Numerical Simulation of Temperature Field of Vertical Core-Filling Continuous

Casting for Cu/Al/C_f Composites *Foundry* 65 (6) 2016: pp. 527 – 532. https://doi.org/10.3969/j.issn.1001-4977.2016.06.008

16. **Yu, C.X..** Engineering Heat Transfer. Emenshan: Southwest Jiaotong University Press; 1990: pp. 128 – 139.
17. **Yang, S.M., Tao, W.Q.** Heat Transfer. Beijing: Higher Education Press; 2006: pp. 277 – 281.
18. **ASTM D5470-17**. Standard Test Method for Thermal Transmission Properties of Thermally Conductive Electrical Insulation Materials. West Conshohocken, PA, USA: ASTM International, 2017.
19. **Liu, X.H., Fu, H.D., He, X.Q., Fu,X.D., Jiang, Y.Q., Xie, J.X.** Numerical Simulation Analysis of Continuous Casting Cladding Forming of Cu-Al Composites *Acta Metallurgica Sinica* 54 (3) 2018: pp. 470 – 484. https://doi.org/CNKI:SUN:JSXB.0.2018-03-014
20. **Liu, X.H., Fu, X.T., Fu, H.D., Xie, J.X.** Numerical Simulation Analysis of Effects Of Processing Parameters on Forming Process of Vertical Continuous Core-Filling Casting for Copper Clad Aluminum Billets With Large Section *The Chinese Journal of Nonferrous Metals* 27 (3) 2017: pp. 514 – 524. https://doi.org/10.19476/j.ysxb.1004.0609.2017.03.009
21. **Strzępek, P., Mamala, A., Boumerzoug, Z.** Effect of Horizontal Continuous Casting Parameters on Cyclic Macrosegregation, Microstructure, and Properties of High-Strength Cu–Mg Alloy Cast Rod *Metallurgical and Materials Transactions A* 56 (1) 2025: pp. 41 – 60. https://doi.org/10.1007/s11661-024-07645-9
22. **Cai, K.K., Cheng, S.F.** Principles and Technology of Continuous Casting of Steel Beijing: Metallurgical Industry Press, 1994: pp. 56 – 60.
23. **Liu, Y.L.** Analysis on Disturbance Mechanism of Liquid Metal in Horizontal Continuous Casting *Special Casting & Nonferrous Alloys* 6 1994: pp. 34 – 36. https://doi.org/CNKI:SUN:TZZZ.0.1994-06-013
24. **Liu, N., Guo, L.L., Zhang, X.W.** Study on the Influence of Horizontal Continuous Casting Process on the Surface Quality of Cu-15Ni-8Sn Alloy Sheet *Journal of Qilu University of Technology* 36 (5) 2022: pp. 44 – 50. https://doi.org/ 10.16442/j.cnki.qlgydxxb.2022.05.007
25. **Lv, W., Zhao, Y.H., Liang, H.B.** Key Techniques for Realizing High-Speed Continuous Casting *Journal of Shenyang Institute of Aeronautical Engineering* 16 1999: pp. 23 – 26.
26. **Liu, J.P., Liu, X.S., Huang, H.Y., Xie, J.X.** Maximum Steady-State Drawing Velocity of Cu-12%Al Wires During OCC *The Chinese Journal of Nonferrous Metals* 2 2011: pp. 171 – 178. https://doi.org/10.1631/jzus.A1000150
27. **Zhao, J.S., Zhang, Y.B.** Effect of Draw Speed on Solidification of Bloom in Continuous Casting *Journal of Inner Mongolia University of Science and Technology* 2007: pp. 46 – 49. https://doi.org/ 10.3969/j.issn.2095-2295.2007.01.012
28. **Yi, H., Zhang, X.B., Yu, E.L., Lei, S.** Numerical Analysis of Temperature Field and Structure Field in Horizontal Continuous Casting Process for Copper Pipes *International Journal of Heat and Mass Transfer* 115 2017: pp. 294 – 306. https://doi.org/10.1016/j.ijheatmasstransfer.2017.08.037
29. **Zong, F.C., Ge, S.J., Qian, W.T., Yuan, G.L., Liu, Y.C.** Effect of Alloy Elements and Pouring Temperature on Shrinkage and Fluidity of $AlSi_9Cu_3$ Alloy *Hot Working Technology* 50 2021: pp. 45 – 47.
30. **Shi, S., Yan, J., Fan, W.Z.** Effect of Pouring Temperature on Mechanical Properties and Thermal Conductivity of Gravity Cast Al-10Si-0.3Mg Alloy *Foundry* 70 2021: pp. 695 – 699. https://doi.org/ CNKI:SUN:TZZZ.0.2014-05-013
31. **Shuai, G.W., Zhang, M., Ding, Y.** Effect of Vacuum Casting Process on Microstructure and Properties of Cu-Cr Alloy *Materials Science and Technology* 1 2007: pp. 68 – 71. https://doi.org/ 10.3969/j.issn.1005-0299.2007.01.017
32. **Li, Y.M., Duan, W.C., Li,W.S., Zhang, R.Q.** Effect of Foundry Heat Treatment on Properties of CuCr0.9 Alloys *Hot Working Technology* 42 (11) 2013: pp. 33 – 35. https://doi.org/CNKI:SUN:SJGY.0.2013-11-009
33. **Long, H.S., Zhang, Y., Liu, J.S., Chen, D.X., Song, H.W.** Optimization of Primary Cooling Structure for TP2 Copper Tube Billets in Horizontal Continuous Casting Based on Finite Element Simulation *Copper Engineering* 2 2024: pp. 8 – 17.
34. **Sun, Y.Q., Pan, J.Q., Chen, J.B., Chen, L.Z., Zhao, J.L., Gao, J.H.** Influence of Process Parameters on Microstructure of Upward Continuous Casting Cu-Mg Alloy Bar *Nonferrous Metals Engineering* 7 (5) 2017: pp. 16 – 19. https://doi.org/10.3969/j.issn.2095-1744.2017.05.004
35. **Zhao,R.L., Liu, Y., Tian, B.H., Zhang, X.W., Zhang, Y.** High Temperature Deformation Behavior of Pure Copper *Heat Treatment of Metals* 36 (8) 2011: pp. 17 – 20. https://doi.org/CNKI:SUN:JSRC.0.2011-08-005
36. **Wang, J.** Study on High-Temperature Deformation Behavior and Microstructure Evolution of Pure Copper, Harbin Institute of Technology, PhD thesis, 2020.
37. **Zhao, D.J.** Study on the Formation Mechanism and Technology Control of the Cracks and Holes in the Continuous Casting Copper Bar *Copper Engineering* 2 2013: pp. 1 – 4. https://doi.org/CNKI:SUN:TYGC.0.2013-02-003
38. **Zhang, Z.Y.** Discussion on the Theory of Dummy Bar for Horizontal Continuous Casting *Heavy Machinery* 10 1981: pp. 6 – 10+5. https://doi.org/CNKI:SUN:ZXJX.0.1981-10-001